# Dynamical behaviors of discretized second-order terminal sliding-mode control systems

Galias, Zbigniew; Yu, Xinghuo



Galias, Z., & Yu, X. (2012). Dynamical behaviors of discretized second-order terminal sliding-mode control systems. IEEE Transactions on Circuits and Systems 2- Express Briefs, 59(9), 597–601.
https://doi.org/10.1109/TCSII.2012.2206930
Document Version: Accepted Manuscript

Published Version: https://doi.org/10.1109/TCSII.2012.2206930

# Dynamical Behaviors of Discretized Second-Order Terminal Sliding Mode Control Systems

Zbigniew Galias, *Member, IEEE,* Xinghuo Yu, *Fellow, IEEE*

***Abstract*—Discretization behaviors of second order terminal sliding mode control systems are studied. The existence, stability and basins of attraction of periodic solutions are investigated. The influence of system's parameters on the size of the steady state solution is discussed. Theoretical results are illustrated with simulation examples.**

***Index Terms*—Sliding mode control, discretization, periodic solution, basin of attraction.**

## I. Introduction

Sliding mode control (SMC) has been widely studied and used for many years due to its simplicity and robustness in systems variations and disturbances [1]. The essence of SMC is the peculiar 'sliding' motion induced by discontinuous control (called 'sliding mode'), which enables the system trajectory to reach and stay in a prescribed switching manifold indefinitely. This results in insulation of the controlled system from certain external disturbances, assuming infinite switching capacity of the control devices. However, modern industrial control systems are implemented digitally, which means industrial SMC would be executed in discrete-time. The digitization scale becomes a factor affecting the control performance. For example, irregular behaviors such as periodic trajectories and strange attractors were reported in [2], [3].

Terminal sliding mode control (TSMC) is a new class of SMC which employs a nonlinear switching manifold to achieve the finite-time convergence [4], delivering superior tunable finite time global stability and robustness. Recently, this control has been studied substantially and used in practical applications [5]. However, little is known about discretization behaviors in TSMC systems apart from an early work [6], and [7]. It is of practical importance to understand these behaviors in order to develop strategies to improve control performance in digital implementations of TSMC.

In this paper, we study the second order TSMC discretized using the simplest discretization method — the Euler method. Various dynamical phenomena are described. Complete classification of the period–2 orbits is given and the influence of system's parameters on their size is studied. Basins of attraction of period–2 and period–4, which are the only two types of steady states observed in simulations, are investigated. This analysis reveals the underpinning generation mechanism of periodic orbits, which will help develop effective discrete-time TSMC with less chattering and better robustness. In simulation examples, it is shown that the fractional power used in TSMC gives rise to richer dynamical behaviors such as multiple attractors, fractal basins, and bursts in time waveforms.

This work was supported in part by the AGH University of Science and Technology, grant no. 11.11.120.611 and under the Australian Research Councils Discovery Grant Scheme, project no. DP0986376.

Z. Galias is with the AGH University of Science and Technology, Dept. of Electrical Eng., 30–059, Kraków, Poland (e-mail: galias@agh.edu.pl).

X. Yu is with the School of Electrical and Computer Engineering, RMIT University, Melbourne, VIC 3001, Australia (e-mail: x.yu@rmit.edu.au).



## II. Euler discretization of second-order terminal sliding mode control systems

Let us consider a single input two-dimensional linear system in the controllable canonical form

$$\dot{x} = Ax + bu = \begin{pmatrix} 0 & 1 \\ -a_1 & -a_2 \end{pmatrix} \begin{pmatrix} x_1 \\ x_2 \end{pmatrix} + \begin{pmatrix} 0 \\ 1 \end{pmatrix} u, \qquad (1)$$

and the terminal sliding mode control

$$u(x) = a_1 x_1 + a_2 x_2 - \beta r x_1^{r-1} x_2 - \alpha \operatorname{sgn}(x_2 + \beta x_1^r), \qquad (2)$$

where $\operatorname{sgn}(y) = 1$ for $y \geq 0$, $\operatorname{sgn}(y) = -1$ for $y < 0$, $r = q/p \in (0.5, 1)$, $q$ and $p$ are odd positive integers, $\alpha > 0$, $\beta > 0$. Let us note that $x^r = \operatorname{sgn}(x)|x|^r$, and $x^{r-1} = |x|^{r-1}$. We consider the effects of digital implementation of the above control system by Euler discretization at moments $t_k = kh$, where $h > 0$ is the discretization step. Let us denote $z(k) = (z_1(k), z_2(k)) = (x_1(kh), x_2(kh))$. A trajectory $(z(0), z(1), \ldots)$ is associated with its symbol sequence $s = (s_0, s_1, \ldots)$, where $s_k = \operatorname{sgn}(z_2(k) + \beta z_1(k)^r)$. The update equation for the discrete system is $z(k+1) = f(z(k))$, where the map $f$ is defined as

$$f(z_1, z_2) = \left(z_1 + h z_2, (1 - h\beta r z_1^{r-1}) z_2 - h\alpha s_k\right). \qquad (3)$$

## III. Study of Dynamical Behaviors

It is clear that for discretized SMC systems trajectories cannot converge to the origin. Due to the discrete nature of the control action the best steady state behavior which can be obtained is a period–2 orbit with the size converging to zero when the discretization step goes to zero. This desired property of the discretized SMC system has been confirmed for $r = 1$ [8]. It has been shown that when $h < 2/\beta$ the system is stable and all trajectories converge to a period–2 orbit with $|z_2| = \alpha h/(2 - h\beta)$, and $|z_1| \leq \alpha h/(\beta(2 - h\beta))$. A key property for $r = 1$ is that once there is a symbol change the symbols will alternate forever. Simulations indicate that for $r < 1$ trajectories converge either to a period–2 orbit or a period–4 orbit. It is therefore important to study the existence and properties of short periodic orbits.

We say that $z$ is a *period–p point* if $f^p(z) = z$ and $f^k(z) \neq z$ for $k = 1, 2, \ldots, p-1$. We say that a periodic symbol sequence

$s=(s_0,s_1,\ldots,s_{p-1})$ is *admissible* if there exists a period–$p$ point $z(0)$ with the symbol sequence $s$.

First, let us note that if $z(0)$ is a period–$p$ point then $z_2(0)+z_2(1)+\cdots+z_2(p-1)=0$. This follows from $z_1(p)=z_1(0)+h(z_2(0)+z_2(1)+\cdots+z_2(p-1))$.

Clearly, there are no fixed points (period–1 orbits) of $f$. Indeed, the conditions $z_1(0)=z_1(0)+hz_2(0)$ and $z_2(0)=(1-h\beta r z_1(0)^{r-1})z_2(0)-h\alpha s_0$ are contradictory.

### A. Period–2 orbits

The following lemma provides conditions for the existence of period–2 orbits.

*Lemma 1:* Each period–2 orbit is of the form $(\xi,-2\xi/h)$, $(-\xi,2\xi/h)$ where

$$v(\xi)=2\xi-h\beta r\xi^r-0.5h^2\alpha=0, \tag{4}$$

$$\xi<0.25h^2\alpha/(1-r). \tag{5}$$

The orbit is asymptotically stable if and only if $|\xi|>\eta=(0.5h\beta r^2)^{1/(1-r)}$.

*Proof:* The symbol sequence $s=(s_0,s_1)$ is admissible if and only if the set of equations $z_1(1)=z_1(0)+hz_2(0)$, $z_1(0)=z_1(1)+hz_2(1)$, $z_2(1)=(1-h\beta r z_1(0)^{r-1})z_2(0)-h\alpha s_0$, $z_2(0)=(1-h\beta r z_1(1)^{r-1})z_2(1)-h\alpha s_1$, has a solution satisfying $s_0=\mathrm{sgn}(z_2(0)+\beta z_1(0)^r)$, $s_1=\mathrm{sgn}(z_2(1)+\beta z_1(1)^r)$. Eliminating $z_2(0)=(z_1(1)-z_1(0))/h$ and $z_2(1)=(z_1(0)-z_1(1))/h$ and using the notation $z_{10}=z_1(0)$ and $z_{11}=z_1(1)$ yields

$$\left(2-h\beta r z_{10}^{r-1}\right)(z_{11}-z_{10})=h^2\alpha s_0, \tag{6a}$$

$$\left(2-h\beta r z_{11}^{r-1}\right)(z_{11}-z_{10})=-h^2\alpha s_1, \tag{6b}$$

$$s_0=\mathrm{sgn}(z_{11}-z_{10}+h\beta z_{10}^r), \tag{6c}$$

$$s_1=\mathrm{sgn}(z_{10}-z_{11}+h\beta z_{11}^r). \tag{6d}$$

First, we will show that period–2 sequence with $s_0=s_1$ is not admissible. This is expected, as otherwise the corresponding trajectory would stay forever on one side of the sliding surface. We will consider the case $s_0=s_1=+1$. For the opposite case the results can be obtained in the same way. From (6a) it follows that $z_{10}\neq z_{11}$. Without loss of generality we can assume that $z_{11}>z_{10}$. With this assumption, it follows from (6d) that $z_{11}$ is positive. Since $z_{11}-z_{10}>0$ it follows from (6b) that $2-h\beta r z_{11}^{r-1}<0$ and in consequence $|z_{11}|<(0.5h\beta r)^{1/(1-r)}$. Since $z_{11}$ is positive, it follows that

$$0<z_{11}<(0.5h\beta r)^{1/(1-r)}. \tag{7}$$

Since $z_{11}-z_{10}>0$ it follows from (6a) that $2-h\beta r z_{10}^{r-1}>0$ and in consequence $|z_{10}|>(0.5h\beta r)^{1/(1-r)}$. Since $z_{10}<z_{11}<(0.5h\beta r)^{1/(1-r)}$ and $|z_{10}|>(0.5h\beta r)^{1/(1-r)}$ we obtain

$$-z_{10}>(0.5h\beta r)^{1/(1-r)}. \tag{8}$$

From (7,8) it follows that $0<z_{11}<-z_{10}$, and $z_{11}^r<-z_{10}^r$. Finally, taking into account (6c,6d) we obtain $z_{11}-z_{10}\leq h\beta z_{11}^r<-h\beta z_{10}^r\leq z_{11}-z_{10}$, which is a contradiction.

It remains to consider the case $(s_0,s_1)=(-1,+1)$. The opposite symbol sequence leads to the same periodic orbits. From (6a,6b), taking into account that $z_{10}\neq z_{11}$, we obtain $z_{10}^{r-1}=z_{11}^{r-1}$. It follows that $|z_{10}|=|z_{11}|$. Since $z_{10}\neq z_{11}$ it follows that $z_{11}=-z_{10}$, and eliminating $z_{11}$ from (6a) yields $2z_{10}-h\beta r z_{10}^r-0.5h^2\alpha=0$. Hence $z_{10}$ is a zero of $v$ and $z_{20}=(z_{11}-z_{10})/h=-2z_{10}/h$.

To prove the first part of the lemma, it remains to find conditions ensuring that inequalities (6c,6d) hold. Let us note that since $-z_{11}=z_{10}=\xi\neq 0$, (6d) follows from (6c) and it is sufficient to prove that $-2\xi+h\beta\xi^r<0$ is equivalent to $\xi<0.25h^2\alpha/(1-r)$. Since $v(\xi)=0$, it follows that $h\beta r\xi^r=2\xi-0.5h^2\alpha$. Inserting $h\beta\xi^r=(2\xi-0.5h^2\alpha)/r$ into $-2\xi+h\beta\xi^r<0$ gives the upper bound on $\xi$ as in (5).

The Jacobian matrix of $f$ at $z=(z_1,z_2)$ is

$$J(z_1,z_2)=\begin{pmatrix}1 & h\\ -h\beta r(r-1)z_1^{r-2}z_2 & 1-h\beta r z_1^{r-1}\end{pmatrix}.$$

The orbit is asymptotically stable if and only if all eigenvalues of the matrix $J(-\xi,2\xi/h)J(\xi,-2\xi/h)$ lie within the unit circle. Since $J(\xi,-2\xi/h)=J(-\xi,2\xi/h)$ it is sufficient to study eigenvalues of

$$J(\xi,-2\xi/h)=\begin{pmatrix}1 & h\\ 2\beta r(r-1)\xi^{r-1} & 1-h\beta r\xi^{r-1}\end{pmatrix}.$$

The characteristic equation of this matrix is $\lambda^2+\lambda(h\beta r\xi^{r-1}-2)+1-h\beta r\xi^{r-1}(2r-1)=0$. According to the Jury's criterion, the second order polynomial $F(\lambda)=\lambda^2+a_1\lambda+a_0$, has all zeros within the unit circle if and only if (a) $a_0<1$, (b) $a_0+a_1+1>0$, and (c) $a_0-a_1+1>0$. The first condition is equivalent to $h\beta r\xi^{r-1}(2r-1)>0$ and is always satisfied since $\xi^{r-1}$ is positive and $2r>1$. Since $a_0+a_1+1=2h\beta r(1-r)\xi^{r-1}>0$ the second condition also holds. The third condition $1-h\beta r\xi^{r-1}(2r-1)+2-h\beta r\xi^{r-1}+1>0$ is equivalent to $|\xi|>\left(0.5h\beta r^2\right)^{1/(1-r)}$. ∎

Let us define two quantities:

$$h_1=h_1(r)=(0.25\alpha r/(1-r))^{\frac{1-r}{2r-1}}(0.5\beta)^{-1/(2r-1)}, \tag{9}$$

$$h_2=h_2(r)=(0.25\alpha r/(1-r))^{\frac{1-r}{2r-1}}(0.5\beta r^2)^{-1/(2r-1)}. \tag{10}$$

The following theorem gives complete classification of period–2 solutions.

*Theorem 1:*
1) If $h<h_1$ then there exists a single period–2 orbit $(\xi,-2\xi/h),(-\xi,2\xi/h)$ where $\xi>\eta=(0.5h\beta r^2)^{1/(1-r)}$ is the only zero of $v$. The orbit is asymptotically stable.
2) If $h\in[h_1,h_2)$ then there are no period–2 orbits.
3) If $h=h_2$ then there is one period–2 orbit $(\xi,-2\xi/h),(-\xi,2\xi/h)$, where $\xi=-\eta$. The orbit is not asymptotically stable.
4) If $h>h_2$ then there are two period–2 orbits $(\xi_{1,2},-2\xi_{1,2}/h),(-\xi_{1,2},2\xi_{1,2}/h)$, where $\xi_1<-\eta<\xi_2$ are the two negative zeros of $v$. The orbit corresponding to $\xi_1$ is stable, the other one is unstable.

*Proof:* First, let us study the number of zeros of $v$ depending on $h$. Since $r<1$, it follows that $\lim_{x\to\pm\infty}v(x)=\pm\infty$. The derivative $v'(x)=2-h\beta r^2x^{r-1}$ vanishes at $x=\pm\eta=\pm(0.5h\beta r^2)^{1/(1-r)}$. $v(\eta)$ is negative. $v(-\eta)$ is negative when $-2\eta+h\beta r\eta^r<0.5h^2\alpha$, which is equivalent to $h<h_2$.

It follows that for $h<h_2$, $h=h_2$, and $h>h_2$ the function $v$ has one, two, and three zeros, respectively.

For $h<h_2$ the function $v$ has a single zero $\xi\in(\eta,\infty)$. From Lemma 1 it follows that $\xi$ defines a period–2 orbit if

$\xi < 0.25h^2\alpha/(1-r)$, which is equivalent to $h < h_1$. It follows that if $h < h_1$ then $\xi$ defines a period–2 orbit. For $h \in [h_1, h_2)$ we have $\xi \geq 0.25h^2\alpha/(1-r)$ and $\xi$ does not define a period–2 orbit. This completes proof of assertions 1 and 2.

When $h = h_2$ there are two zeros of $v$, one is positive, and the second one is $-\eta$. Since $h_2 > h_1$ the positive solution does not define a period-2 orbit. The negative solution satisfies (5) and hence it defines a period–2 orbit.

When $h > h_2$ there are three zeros of $v$. As in the previous case the positive solution does not define an orbit. Both negative solutions define a period–2 orbit.

Assertions about stability follow from Lemma 1. ■

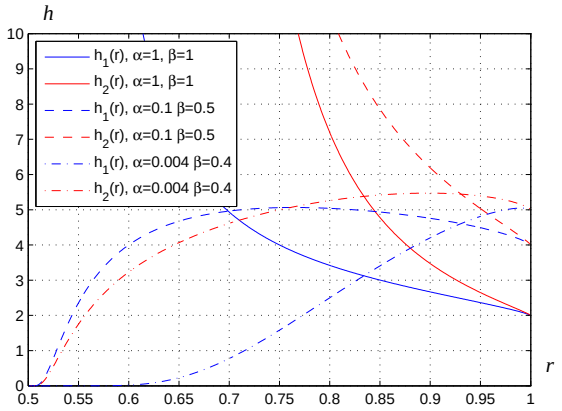


Fig. 1. Existence of period–2 orbits, plots of $h_1(r)$ and $h_2(r)$, $h_1(r) \leq h_2(r)$; (a) $\alpha = 1$, $\beta = 1$, (b) $\alpha = 0.1$, $\beta = 0.5$, (c) $\alpha = 0.04$, $\beta = 0.4$

Now, let us study how the range of integration steps for which period–2 orbit exists changes with $r$, i.e. we study functions $h_1(r)$ and $h_2(r)$ with fixed $\alpha$ and $\beta$. Let us note that $h_1(r) < h_2(r)$ for all $r \in (0.5, 1)$. Moreover $\lim_{r\to 1^-} h_1(r) = \lim_{r\to 1^-} h_2(r) = 2/\beta$. The limits at $r = 0.5^+$ change at critical values $\alpha = \beta^2/32$ and $\alpha = \beta^2/2$, more precisely $h_1(0.5^+) = 0$ for $\alpha < \beta^2/32$, $h_1(0.5^+) = \infty$ for $\alpha > \beta^2/32$, $h_2(0.5^+) = 0$ for $\alpha < \beta^2/2$, and $h_2(0.5^+) = \infty$ for $\alpha > \beta^2/2$. Fig. 1 shows the bounds $h_1$ and $h_2$ in three typical cases. For $\alpha = 1$, $\beta = 1$ ($\alpha > \beta^2/2$) the limits are $h_1(0.5^+) = h_2(0.5^+) = \infty$. For $\alpha = 0.5$, $\beta = 0.5$ we have $\beta^2/32 < \alpha < \beta^2/2$, and $h_1(0.5^+) = 0$, $h_2(0.5^+) = \infty$, while for $\alpha = 0.004$, $\beta = 0.4$ ($\alpha < \beta^2/32$) we have $h_1(0.5^+) = h_2(0.5^+) = 0$.

Since $h_1(r) > 0$, it follows that for sufficiently small $h$ there always exists a single period–2 orbit, but the bound $h_1(r)$ can be very small when $r$ is close to 0.5 (compare Fig. 1).

We have shown that for $h < h_1$ there exists a single period–2 orbit $(\xi, -2\xi/h), (-\xi, 2\xi/h)$ where $\xi$ is the only zero of $v$. Let us now study how the size $\xi(r)$ of period–2 orbit depends on $r$. For $r = 1$ and $r = 0.5$ one can solve (4) analytically: $\xi(1) = 0.5h^2\alpha/(2-h\beta)$, $\xi(0.5) = h^2(\beta + \sqrt{\beta^2 + 16\alpha})^2/64$.

Below, we show that for sufficiently small $h$ the size of the orbit grows when $r$ decreases.

*Lemma 2:* Let $h > 0$, and $0.5 < r_1 < r_2 < 1$ be such that $h_1(r) > h$ for $r \in [r_1, r_2]$. If $h < h_3 = 8\mathrm{e}^{-1}\left(\beta + \sqrt{\beta^2 + 16\alpha}\right)^{-1}$ then $\xi(r)$ in the interval $[r_1, r_2]$ is strictly decreasing.

*Proof:* $\xi(r)$ satisfies the equation $2\xi - h\beta r\xi^r - 0.5h^2\alpha = 0$. From the implicit function theorem it follows that $\xi'(r) = h\beta\xi^r(1 + r\ln\xi)/(2 - h\beta r^2\xi^{r-1})$. From (6a) it follows that $2 - h\beta r\xi^{r-1} > 0$. Since $0.5 < r < 1$ it follows that the denominator is positive. Therefore, the condition that $\xi(r)$ is strictly decreasing is equivalent to $1 + r\ln\xi < 0$, or $\xi(r) < \mathrm{e}^{-1/r}$. Since the function $\mathrm{e}^{-1/r}$ is increasing and $[r_1, r_2] \subset (0.5, 1)$, it is sufficient that the condition is satisfied for $r = 0.5$, i.e. $h^2/64\left(\beta + \sqrt{\beta^2 + 16\alpha}\right)^2 < \mathrm{e}^{-2}$. ■

The above lemma states that for $h < h_3$ the size of the period–2 orbit increases when $r$ is reduced. This means that the control result deteriorates assuming that trajectories converge to the period–2 solution.

One can also show that for large $h$ ($h > h_4 = (\sqrt{\beta^2 + 4\alpha\mathrm{e}} - \beta)/(\alpha\mathrm{e})$) the opposite situation takes places — the size of the orbit decreases when $r$ is reduced.

### B. Period–4 orbits

In simulations one observes that some trajectories converge to a self symmetric ($z(2) = -z(0)$) period–4 orbit with the symbol sequence $s = (-1, -1, +1, +1)$. Let us denote the orbit by $((z_{10}, z_{20}), (z_{11}, z_{21}), (-z_{10}, -z_{20}), (-z_{11}, -z_{21}))$. The conditions for the existence of such periodic orbit are: $z_{11} = z_{10} + hz_{20}$, $-z_{10} = z_{11} + hz_{21}$, $z_{21} = z_{20} - h\beta r z_{10}^{r-1} z_{20} + h\alpha$, $-z_{20} = z_{21} - h\beta r z_{11}^{r-1} z_{21} + h\alpha$, $z_{20} + \beta z_{10}^r < 0$, $z_{21} + \beta z_{11}^r < 0$.

In the following lemma, the problem of existence of these orbits is reformulated as a problem of existence of zeros of a one-dimensional map with certain constrains.

*Lemma 3:* Let us assume that $h \neq (0.5\alpha)^{(1-r)/(2r-1)}(0.5\beta r)^{-1/(2r-1)}$. $((z_{10}, z_{20}), (z_{11}, z_{21}), (-z_{10}, -z_{20}), (-z_{11}, -z_{21}))$ is a self symmetric period–4 orbit with the symbol sequence $(-1, -1, +1, +1)$ if and only if $v_4(z_{10}) = (2z_{10} - h^2\alpha)(2z_{10}^{1-r} - h\beta r)^r(h\beta r z_{10}^r + h^2\alpha)^{1-r} + h\beta r z_{10}^{r(1-r)}(2h\beta r z_{10}^r + h^2\alpha - 2z_{10}) = 0$, $z_{11} = -(h\beta r z_{10}^r + h^2\alpha)/(2 - h\beta r z_{10}^{r-1})$, $z_{11} - z_{10} + h\beta z_{10}^r < 0$, $-z_{10} - z_{11} + h\beta z_{11}^r < 0$, $z_{20} = (z_{11} - z_{10})/h, z_{21} = (-z_{11} - z_{10})/h$.

In the proof, which is very technical, one uses methods similar to the ones used in the proof of Lemma 1. This lemma is used in the next section to find regions where symmetric period–4 orbits exist.

### C. Evaluation of the inverse map

The map $f$ is not defined over the set $\Omega = \{(z_1, z_2) : z_1 = 0\}$, called in the following the *singular line*. Trajectories, which come very close to this line are repelled from the origin. Another important set in the state space is the *discontinuity line* $S = \{(x_1, x_2) : s(x) = x_2 + \beta x_1^r = 0\}$, where $f$ is not continuous.

These two lines and their preimages split the state space into regions. The closer the trajectory comes to a border between these regions the more difficult it is to predict its behaviour in the future. In this section, we describe a procedure for the evaluation of the inverse map, which is later used to study the sets $f^{-k}(\Omega)$ and $f^{-k}(S)$.

Let us consider the multivalued transformation $g = f^{-1}$ inverse to the transformation $f$ defined in (3). The point $z = (z_1, z_2)$ belongs to $f^{-1}(y_1, y_2)$ if and only if $y_1 = z_1 + hz_2$, $y_2 = (1 - h\beta r z_1^{r-1})z_2 - h\alpha s$, and $s = \mathrm{sgn}(z_2 + \beta z_1^r)$. Eliminating $z_2 = (y_1 - z_1)/h$ yields

$$r_s(z_1) = z_1 + h\beta r z_1^{r-1} y_1 - h\beta r z_1^r + h y_2 + h^2\alpha s - y_1 = 0. \quad (11)$$

The numerical procedure for finding $g(z)$ is following. For $s=\pm 1$ solve (11) numerically obtaining a set of possible values for $z_1$. If $s=\operatorname{sgn}(z_2+\beta z_1^r)$ where $z_2=(y_1-z_1)/h$, then $(z_1,z_2)\in f^{-1}(y_1,y_2)$. The most difficult part of this procedure is solving (11). The problem can be greatly simplified by finding monotonicity intervals of $r_s$. Once they are known, one can easily locate zeros of $r_s$. If $r_s$ evaluated at interval endpoints are of opposite signs, then there exist exactly one solution in this interval, and one can locate it using any general method for finding a bracketed root. In the opposite case there are no solutions in this interval.

Since $r_s(-z_1,-y_1)=-r_s(z_1,y_1)$ without loss of generality we may assume that $y_1\geq 0$. When $y_1=0$ the function $r_s(z_1)=z_1-h\beta r z_1^r+hy_2+h^2\alpha s$ is continuous and has two local extrema at $\gamma_{1,2}=\mp(h\beta r^2)^{1/(1-r)}$. The monotonicity intervals are $(-\infty,\gamma_1)$, $(\gamma_1,\gamma_2)$, and $(\gamma_2,\infty)$.

For $y_1\neq 0$, local extrema of $r_s$ satisfy the condition $t(z_1)=z_1^{2-r}-h\beta r(1-r)y_1-h\beta r^2 z_1=0$. Endpoints of monotonicity intervals for $r_s$ are zeros of $t$, $\pm\infty$, and $0^{\pm}$. Zeros of $t$ can be easily found numerically by using the fact that $t$ has local extrema at $\pm\left((h\beta r^2)/(2-r)\right)^{1/(1-r)}$.

## IV. Case Study

In this section, we analyse in detail dynamical phenomena for the case $\beta=1$, $\alpha=1$.

First, let us study the problem of existence of periodic orbits. Using Theorem 1, we have found regions in the $(h,r)$ plane where stable period–2 orbits exist (see Fig. 2(a)).

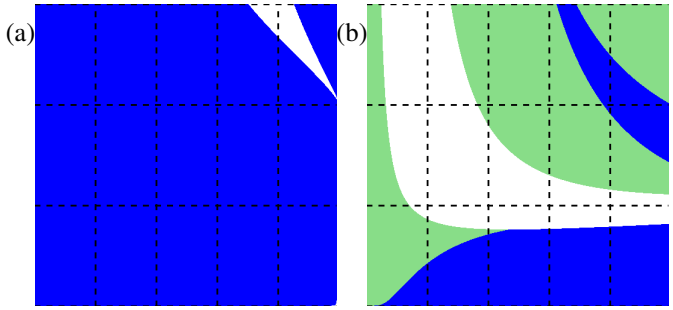


Fig. 2. $\alpha=1$, $\beta=1$, $r\in[0.5,1)$, $h\in[0,3]$, (a) period–2 orbits, (b) period–4 orbits; stable orbits — dark blue, unstable orbits — light green

To study the problem of existence of period–4 orbits $500\times 500$ pairs of parameters $(r,h)$ in the region $[0.501,0.995]\times[0.0001,3.0]$ have been selected. For each pair $(r,h)$ Lemma 3 has been used to find whether a symmetric period–4 orbit exists. The results are shown in Fig. 2(b). Pairs $(r,h)$ for which a stable and unstable symmetric period–4 orbit exists are plotted in dark blue and light green, respectively. Notice that stable period–4 orbits exist for all $r$ when $h$ is sufficiently small. The existence region is smaller than for period–2 orbits.

Now, we investigate how the size of periodic solutions changes with $r$. The plot of $z_1$ coordinate of the period–2 orbits versus $r$ for $\alpha=1$, $\beta=1$, $h=0.05<h_3=0.5745$ is shown in Fig. 3(a). The results have been obtained by solving numerically the equation $2\xi-h\beta r\xi^r-0.5h^2\alpha=0$. One can see that when $r$ decreases the size of the orbit increases, as predicted by Lemma 2 for $h<h_3=0.5745$. Note that when the discretization step is small then decreasing $r$ leads to increasing the size of the period–2 orbit thus deteriorating the control performance. The opposite phenomenon for $h>h_4=0.8997$ is shown in Fig. 3(b).

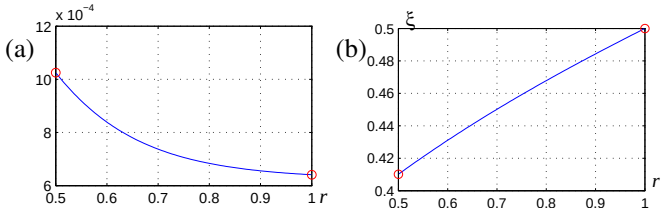


Fig. 3. Size of the period–2 orbit versus $r$; $\alpha=1$, $\beta=1$, (a) $h=0.05<h_3=0.5745$, (b) $h=1.0>h_4=0.8997$.

Let us now compute preimages of singularity and discontinuity lines for $r=0.6$ and $h=0.05$.

In order to find $f^{-k}(\Omega)$ for $k\geq 2$, a number of points belonging to the set $f^{-1}(\Omega)=\{(x_1,x_2)\colon x_1+hx_2=0\}$ is selected and for each point its backward iterates are computed using the algorithm presented in Section III-C. Preimages of $S$ are computed in a similar way. The sets $\Omega$ and $S$ and their preimages $f^{-k}(\Omega)$ and $f^{-k}(S)$ for $k=1,2,\ldots,6$ are plotted in Fig. 4. The sets are symmetric with respect to the transformation $(z_1,z_2)\mapsto(-z_1,-z_2)$.

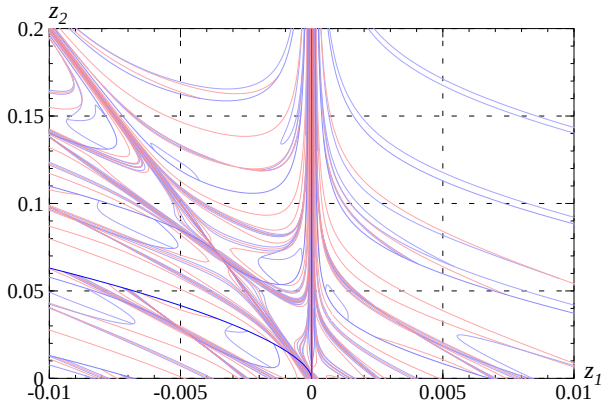


Fig. 4. $\alpha=1$, $\beta=1$, $r=0.6$, $h=0.05$, the singular set $\Omega$ (dark red) and its preimages $g^k(\Omega)$ for $k=1,2,\ldots,6$ (light red), the discontinuity set $S$ (dark blue) and its preimages $g^{-k}(S)$ for $k=1,2,\ldots,6$ (light blue)

One can see that these sets split the state space into narrow regions. Note that if a point belongs to the set $\bigcup_{k=0}^{\infty}f^{-k}(S\cup\Omega)$ then after a finite number of iteration it will hit the discontinuity set or the singularity set. It follows that trajectories may be very sensitive to initial conditions. For points sufficiently close to $f^{-k}(S\cup\Omega)$ it is difficult to predict their future behaviour.

It has been mentioned that in simulations one observes that trajectories converge either to a period–2 orbit or to a symmetric period–4 orbit. In this section this observation is confirmed and basins of attraction of stable periodic orbits are found numerically.

For $r=0.6$ and $h=0.05$ there exist one stable period–2 orbit with the initial point $(-0.00066855,0.0267419)$ and one stable symmetric period–4 orbit with the initial point $(-0.00140679,0.00332914)$. Their basins of attraction are

shown in Fig. 5. Trajectories of $1001 \times 1001$ initial points selected uniformly from the set $(z_1, z_2) \in [-0.01, 0.01] \times [0, 0.2]$ have been computed. 26.04% of trajectories converge to the period–2 orbit and 73.84% converge to the period–4 orbit. The remaining 0.12% of trajectories hit the singularity line.

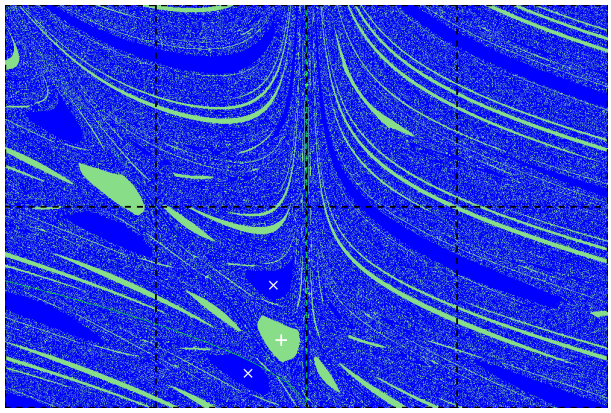

Fig. 5. $\alpha = 1$, $\beta = 1$, $r = 0.6$, $h = 0.05$, $z_1 \in [-0.01, 0.01]$, $z_2 \in [0, 0.2]$, the period–2 ("+") and the period–4 ("×") orbits, basins of attraction of the period–2 orbit (light green) and the period–4 orbit (dark blue)

Note that the boundaries between basins of attraction show a fine fractal structure. Comparing Figs. 4 and 5 one can also note that boundaries between basins are strongly related to preimages of the sets $\Omega$ and $S$.

Similar computations have been carried out for $r = 11/13$, $h = 0.05$. In this case 99.41% and 0.48% of trajectories converge to period–2 and period-4 orbits, respectively. Increasing $r$ makes the basin of attraction of the period–4 orbit smaller. It eventually disappears for $r = 1$.

In order to compare system's trajectories for different $r$ we consider $r_1 = 3/5$, $r_2 = 11/13$, and $r_3 = 1$. In the continuous case for $r < 1$ the relaxation time for the point $(z_1, z_2)$ belonging to the sliding surface is $t_r = |z_1|^{1-r}/(\beta(1-r))$ (compare [4]). For example, $t_{3/5} = 2.5$, $t_{11/13} = 6.5$ for $z_1 = 1$. Example time plots of $z_2$ variable are shown in Fig. 6. In the continuous case trajectories for $r < 1$ reach the origin in finite time (see Fig. 6(a)).

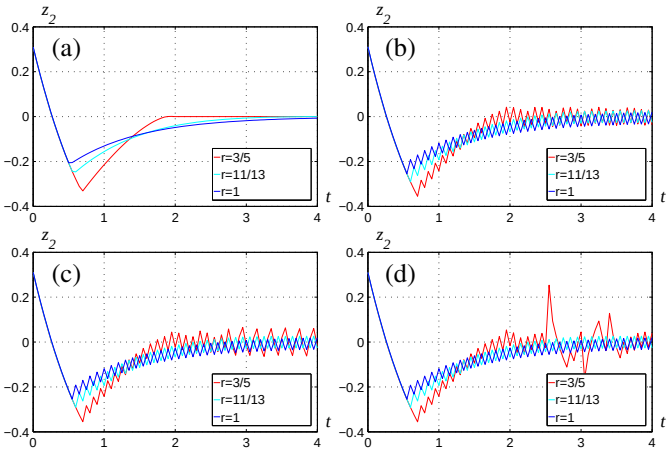


Fig. 6. Example trajectories, $\alpha = 1$, $\beta = 1$, $r \in \{3/5, 11/13, 1\}$ (a) continuous case, $z(0) = (0.2, 0.3109)$, (b) $h = 0.05$, $z(0) = (0.2, 0.3109)$, (c) $h = 0.05$, $z(0) = (0.2, 0.3107)$, (d) $h = 0.05$, $z(0) = (0.2, 0.3102)$

For the initial point $z(0) = (0.2, 0.3109)$ when $h = 0.05$ in all cases trajectories converge to a period–2 orbit. Let us note that the nice property of finite convergence time for TSMC systems is lost when discretization effects are taken into account. In the discrete version infinite time is needed to reach the steady state. It is interesting to note that when $r$ decreases the amplitude of the oscillations grows (see Fig. 6(b)). This is in full agreement with theoretical results (compare Lemma 2).

For the initial point $z(0) = (0.2, 0.3107)$ all trajectories also converge to periodic solutions (see Fig. 6(c)). This time however for $r_1 = 3/5$ the trajectory converges to a period–4 orbit with the amplitude considerably larger.

When the initial point is $z(0) = (0.2, 0.3102)$ one observes several bursts in $z_2$ waveform for the case $r_1 = 3/5$. The bursts are observed in spite of the fact that the initial convergence to the origin is faster than for other values of $r$. Simulations show that such bursts occur for various initial conditions and are associated with the existence of the singular line. When a trajectory comes very close to the line $z_1 = 0$ and $z_2 \neq 0$, then in the next iteration $z_2$ becomes large due to the term $z_1^{r-1}$. Probability of bursts grows when $r$ is decreased.

The examples presented above show also the sensitive dependence to initial conditions. Tiny changes in initial conditions cause drastic changes of trajectories, like convergence to a different steady state, or bursts in time waveforms.

## V. Conclusion

Discretization behaviors in the second order TSMC systems have been studied. Complete results on the existence and stability of period–2 orbits have been presented. It has been shown that for sufficiently small discretization steps the size of the period–2 orbit grows when the parameter $r$ is decreased from 1 thus deteriorating steady state behavior of the control system. It has also been shown that various dynamical behaviors are possible, such as co-existing stable period–2 and period–4 solutions, and basins of attraction with fractal boundaries. Bursts of solutions when converging to the steady state have also been observed. Future work will be focused on extending the findings to higher order TSMC systems.

## References

[1] V. Utkin, *Sliding Modes in Control and Optimization*, ser. Communications and Control Engineering Series. Berlin: Springer Verlag, 1992.

[2] M. di Bernardo and F. Vasca, "Discrete-time maps for the analysis of bifurcations and chaos in DC/DC converters," *IEEE Trans. Circ. Syst. I*, vol. 47, no. 2, pp. 130–143, 2000.

[3] Z. Galias and X. Yu, "Study of periodic solutions in discretized two-dimensional sliding-mode control systems," *IEEE Trans. Circ. Syst. II*, vol. 58, no. 6, pp. 381–385, 2011.

[4] Z. Man and X. Yu, "Terminal sliding mode control of MIMO linear systems," *IEEE Trans. Circ. Syst. I*, vol. 44, no. 11, pp. 1065–1070, 1997.

[5] Y. Wu, B. Wang, and G. Zong, "Finite-time tracking controller design for nonholonomic systems with extended chained form," *IEEE Trans. Circ. Syst. II*, vol. 52, no. 11, pp. 798–802, 2005.

[6] S. Janardhanan and B. Bandyopadhyay, "On discretization of continuous-time terminal sliding mode," *IEEE Trans. Automatic Control*, vol. 51, no. 9, pp. 1532–1536, 2006.

[7] Z. Galias and X. Yu, "Periodic behaviors in discretized second-order terminal sliding mode control systems," in *Proc. European Conference on Circuit Theory and Design*, Linkoping, 2011, pp. 657–660.

[8] ——, "Euler's discretization of single input sliding mode control systems," *IEEE Trans. Automatic Control*, vol. 52, no. 9, pp. 1726–1730, 2007.